

Computational investigation of elastic properties of hypothetical Half-Heusler compounds XNbSn under hydrostatic pressures

R. M. Shabara

*Physics Department, Faculty of Science, Taibah University, Al-Madinah al Munawarah, Saudi Arabia.
Physics Department, Faculty of Science, Damietta University, New Damietta, Egypt.*

B. O. Alsobhi

Physics Department, Faculty of Science, Taibah University, Al-Madinah al Munawarah, Saudi Arabia.

Received 30 October 2022; accepted 4 February 2024

We investigated the electronic, elastic, and magnetic properties of the hypothetical half-Heusler alloys with Niobium base atom, XNbSn with X= Cr, Mn, Co, Fe, V, uses the full-potential (linearized) augmented plane-wave and local-orbitals [FP-(L)APW + lo] basis set in the WIEN2K ab-initio package based on density functional theory (DFT). We investigated the elastic constants, shear modulus, Young modulus, and bulk modulus of these alloys under different pressures (0, 20, 40, and 80 GPa). We predicted that CoNbSn behaves as a semiconductor with a direct energy gap of 0.99 eV, while the other half-Heusler alloys show a metallic behavior. CoNbSn keeps its semiconductor behavior under higher pressures up to 80 GPa. Both VNbSn and CrNbSn have a high value of magnetic moments of 2.158 and 3.002 μ_B , respectively. All XNbSn alloys are stable mechanically at different pressures according to the Born-Huang conditions. CoNbSn, FeNbSn, CrNbSn, and MnNbSn behave as a ductile material at ambient pressure.

Keywords: Half-Heusler; elastic properties; pressure effect; mechanical stability; XNbSn.

DOI: <https://doi.org/10.31349/RevMexFis.70.041002>

1. Introduction

During the last years, there where a significant development in investigating properties of Heusler and half-Heusler alloys and their applications in spintronics and magneto-electronics [1–4]. Several researchers have investigated the structural, electronic, elastic, thermal, and magnetic properties of many Heusler-alloys at ambient pressure and under higher pressures [5–9]. Heusler-alloys are half-metallic materials which may be defined as a new state of matter between insulating and metallic materials. In half-metallic material, the spin-up channel presents metallic behavior, while the spin-down channel exhibits insulating behavior. The polarization of these compounds at Fermi level is 100%. These alloys have many promising applications in spintronics. There are three types of Heusler-alloys: Full-Heusler alloys such as Ru₂MnSb, Ru₂NbSb, Fe₂CrSb, and Co₂CrIn alloys [5, 6]. The second type is half-Heusler alloys such as LaPdBi and ZrCoBi alloys [7, 10], and the third type is Quaternary Heusler-alloys such as CoFeXSb (X=Ru, Zr, Hf, Ta) [11]. Half-Heusler alloys show a high efficiency spintronic application [12, 13], such as magnetic tunneling junctions (MTJs), giant magnetoresistance devices (GMRs), topological insulator, thermoelectric power, and piezoelectric and optoelectronic semiconductors [14–20]. These features make the half-Heusler alloys the most interesting of Heusler-alloy types. It is a common sense to expect that devices using strained materials will not have a long lifetime. To ensure longevity, the material should at least be metastable. There are two conditions for utilizing half-Heusler alloys as device materials, first to be at the optimized lattice constants corre-

sponding to their respective configuration, and second, they should possess a large magnetic moment ($> 3 \mu_B$) with a high Curie temperature.

Recently, Wenfeng Li *et al.* [21] studied the electronic structure and thermoelectric properties of FeNbSb using first principles calculations. They predicted that FeNbSb compound is a promising material for high temperature thermoelectric materials. The structural, electronic, elastic, dynamical, and thermodynamical properties of FeXSb (X=Hf, Nb) compounds were investigated by A. Musari [22]. He predicted that FeNbSb has a semiconductor behavior, while FeHfSb is a half-metallic ferromagnetic compound with a small magnetic moment (0.9 μ_B). The structural, electronic, magnetic, and elastic properties of MnNbZ (Z=As, Sb) and FeNbZ (Z=Sn, Pb) were investigated by Yadav *et al.* [23] using density functional theory. They predicted that the magnetic moment of all the studied compounds is 1 μ_B using GGA and mBJ methods. They also calculated the density of states and band structures of these compounds.

Many half-Heusler alloys have been predicted to be a half-metal at higher pressures and to behave as a metallic material at zero pressure. The half-metallicity of half-Heusler alloys is very sensitive to high pressure as predicted by E. L. Habbak *et al.* [24]. They predicted the absence of half-metallicity of PtCrSb at zero pressure up to 26 GPa, then this material transforms into a half-metallic material with 1 eV energy gap. The stability of these materials under ambient and hydrostatic pressure is very important for feature applications. In this study we introduce a theoretical investigation of the electronic, elastic, and magnetic properties of the hypothetical half-Heusler XNbSn alloys where X= Co, Cr, Fe,

TABLE I. The three possible conventional cubic cell structures of half-Heusler alloys.

	X	Y	Z
Type1	4c (0.25, 0.25, 0.25)	4d (0.75, 0.75, 0.75)	4a (0, 0, 0)
Type2	4a (0, 0, 0)	4d (0.75, 0.75, 0.75)	4c (0.25, 0.25, 0.25)
Type3	4b (0.5, 0.5, 0.5)	4d (0.75, 0.75, 0.75)	4a (0, 0, 0)

Mn, and V atoms. The pressure effect of the elastic properties, bulk modulus, shear modulus, and Young's modulus will be covered in this study using the generalized gradient approximation (GGA) and modified Becke-Johnson (mBJ) [25, 26].

1.1. Theory and computations

This study is a first-principles study of the electronic, elastic, and magnetic properties of hypothetical half-Heusler alloys within the framework of density functional theory (DFT) [27, 28] using the electronic code WIEN2K [29]. This code uses the full-potential (linearized) augmented plane-wave and local-orbitals [$FP - (L)APW + lo$] basis set to solve the Kohn-Sham equations of density functional theory. Our calculations based on the generalized gradient approximation (GGA) and modified Becke-Johnson (mBJ) [25, 26]. In our calculations we used different K-points mesh to reach the most stable optimization curve. The structure of half-Heusler alloys consists of three interpenetrating FCC sublattices followed by one vacant FCC sub-lattice with XYZ formula, where X, Y are transition metals, and Z is the main group element. The half-Heusler XYZ alloys have three possible conventional cubic cell structures as shown in table [1]. In our calculations, we used the crystal structure of type 2 with space group $Fm\bar{3}m(\#216)$, which is the most stable structure for these compounds. The position of atoms in CoNbSn and FeNbSn compounds in the second type crystal structure is shown in Fig.1. In our calculations, we used the following inputs: each atom has specific muffin-tin radius (RMT) of 2.32(X), 2.26(Nb), 2.32(Sn). The commonly used convergence criterion was chosen to be 7 of basis set $K \max \times RMT$, where RMT and $K \max$ are the smallest atomic sphere radius and plane wave cutoff, respectively. The valence wave functions inside the spheres are

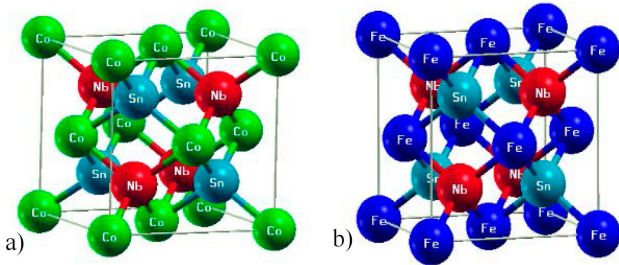


FIGURE 1. Position of atoms in the second type crystal structure of CoNbSn and FeNbSn compounds.

expanded up to $L \max = 10.0$ while the charge density is Fourier expanded up to $G \max = 12(a.u.) - 1$, $K \max = 8.0$. The full Brillouin Zone was sampled by 1728 k-points ($12 \times 12 \times 12$ k-mesh) for self-consistent field (SCF) calculations.

The theoretical values of the equilibrium lattice constant, total and partial magnetic moment, bulk modulus, elastic constants, shear modulus, Young modulus, and Poisson ratio (ν) have been computed in spin polarized calculation within GGA approximation using full potential linearized augmented plane wave (FP-LAPW) method as implemented in the WIEN2k code [29]. Generalized gradient approximation (GGA) has been used for the exchange and correlation effects. The modified Birch-Murnaghan (mBM) equation of state [30, 31] was used in investigation of the bulk modulus and its pressure derivative. To confirm the reliability of our calculations, we must ensure the mechanical stability of these new half-Heusler alloys. There are many methods to check the stability of compounds, such as using the cohesive and formation energies method. Another method to check mechanical stability is using the Born-Huang conditions [32,33] according to the following formulas:

$$C_{11} > 0, \quad C_{44} > 0, \quad C_{11} > C_{12},$$

$$C_{11} + 2C_{12} > 0, \quad C_{12} < B < C_{11}.$$

We used the Born-Huang conditions and calculated the three cubic elastic parameters (C_{11} , C_{12} , and C_{44}), which indicate the stability of these compounds. We used these parameters to calculate other mechanical constants such as bulk modulus (B), Young's modulus (E), shear modulus (G), and Poisson's ratio (ν) according to the following equations.

$$B = \frac{(C_{11} + 2C_{12})}{3}, \quad (1)$$

$$G_V = \frac{(C_{11} - C_{12} + 3C_{44})}{5}, \quad (2)$$

$$G_R = \frac{5C_{44}(C_{11} - C_{12})}{4C_{44} + 3(C_{11} - C_{12})}, \quad (3)$$

$$G = \frac{G_V + G_R}{2}, \quad (4)$$

$$E = \frac{9BG}{3B + G}, \quad (5)$$

$$\nu = \frac{3B - 2G}{2(3B + G)}. \quad (6)$$

TABLE II. The lattice constant, equilibrium volume, bulk modulus, energy gap, total and partial magnetic moments of XNbSn alloys.

XNbSn	a(Ao)	V_0 (a.u. ³)	B(GPa)	B'(GPa)	E_g (eV)	Energy (Ry)	m_x (μ B)	m_{Nb} (μ B)	m_{Sn} (μ B)	m_{total} (μ B)
VNbSn	6.296	420.97	113.952	3.823	0.0	-21897.73685	1.27063	0.36501	-0.00879	2.15803
CrNbSn	6.176	404.011	88.4762	6.969	0.0	-2100.892389	2.62634	-0.09800	0.01631	3.00247
MnNbSn	6.086	391.991	113.746	5.09	0.0	-2316.498951	2.65052	-0.64591	0.01832	1.96550
FeNbSn	6.0199,	371.725	141.441	4.678	0.0	-2544.837730	1.44945	-0.34087	0.00749	1.00244
	6.014[23]	366.969[23]	139.39[23]	5.15[23]	0.239[23]		1.23[23]	-0.22[23]	0.0173[23]	1.00[23]
CoNbSn	5.978	360.717	161.584	3.740	0.990	-2786.238376	0.07851	-0.08089	0.01955	-0.05154

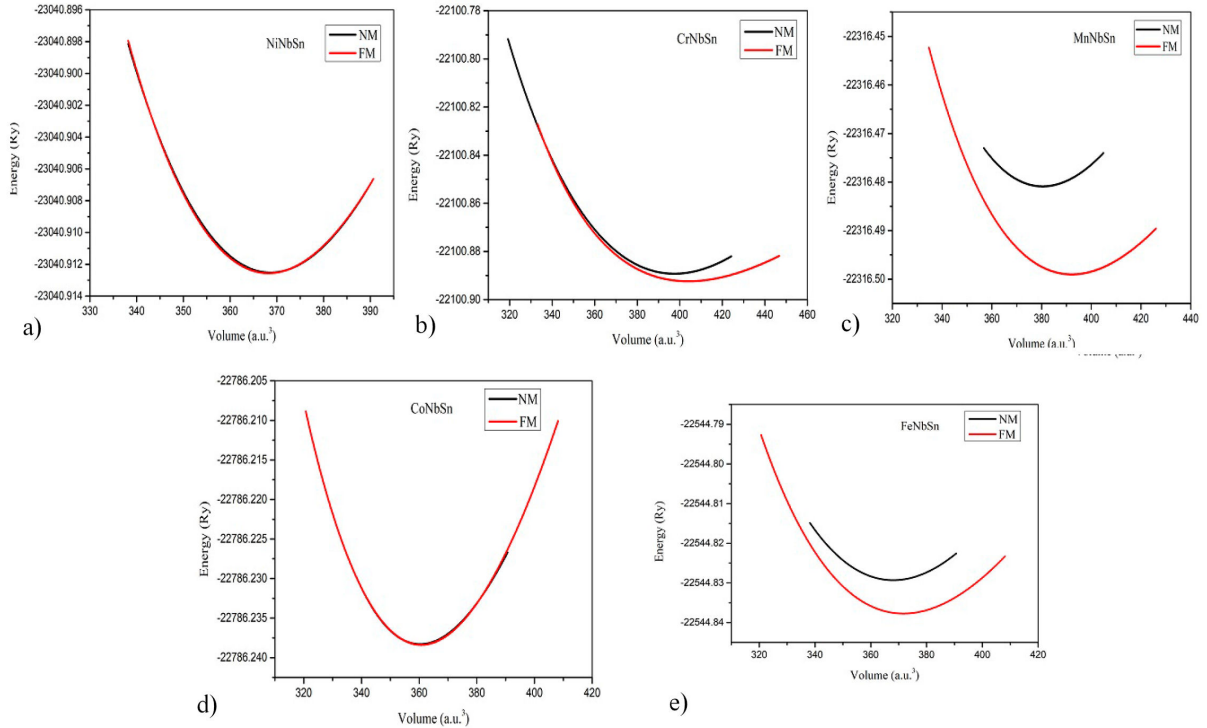


FIGURE 2. Minimization curves of XNbSn (X= Cr, Co, Mn, Ni, and Fe) alloys in both NM and FM states.

2. Result and discussions

2.1. Crystal structure and stability

We have studied the structural, magnetic and elastic properties of XNbSn with (X= Cr, Mn, Co, Fe, V) half-Heusler alloys in the cubic $Fm\bar{3}m(216)$ crystal structure. First, we have examined their energy in ferromagnetic (FM) and nonmagnetic (NM) states as shown in Fig. 2. In CrNbSn, MnNbSn, and FeNbSn materials, the ferromagnetic state is preferred than the nonmagnetic state. In both CoNbSn and NiNbSn, the ferromagnetic and nonmagnetic states have the same energy values, so we can not decide which state is more preferred for these two compounds. These calculations were predicted using the ferromagnetic state. We display in Table II, the calculated lattice constants, minimum volume (V_0), bulk modulus and its pressures derivative calculated from the modified Birch-Murnaghan equation of state [30, 31]. The mag-

netic and partial moments of these compounds are displayed in Table II. We predicted that VNbSn, MnNbSn, FeNbSn and CrNbSn alloys show a metallic behavior with the absence of energy gap at fermi level E_f in both spin-up and spin-down channels. Only CoNbSn alloy presents a semiconductor behavior with an energy gap of 0.99 eV. The presence of this energy gap results from the covalent hybridization between the higher and lower valent elements. Our calculated magnetic moment of FeNbSn shows a good agreement with that calculated by Yadov *et al.* [23]. We predicted that FeNbSn is a metallic alloy with zero energy gap, while Yadov *et al.* [23] calculated an energy gap of 0.239 eV. Up to our knowledge, there is no available data for the other studied alloys to compare with. The presence of Sn atom is crucial to provide stability to these compounds. The spin magnetic moment of the p-orbital of Sn atom is very small compared with other atoms, especially the 3d- atoms. Both VNbSn and

TABLE III. The lattice constant, bulk modulus, shear modulus, Young modulus, and Poisson ratio ν of CoNbSn compound under different pressures.

Pressure(GPa)	A(A0)	Eg(eV)	B*	C_{11} (GPa)	C_{12} (GPa)	C_{44} (GPa)	B(GPa)	G(GPa)	E(GPa)	ν
0	5.977665	0.990	159.019	275.838	100.609	90.615	159.019	89.4025	225.877	0.263259
10	5.871664	1.030	200.362	353.243	119.226	112.753	197.231	114.36	287.672	0.256908
40	5.674468	1.082	301.014	517.014	175.920	174.805	289.618	173.09	433.007	0.250817
80	5.52222	1.103	405.492	680.945	236.618	222.245	384.727	222.12	559.011	0.257832

CrNbSn have a high magnetic moment of 2.158 and 3.002 μ_B , respectively.

3. Pressure effect on elastic properties

The mechanical behavior of crystals, interatomic interaction forces, phase transition mechanism, stability and stiffness of materials could be known from the elastic constants of solids. In ab- initio calculations there are two common methods to obtain the elastic constants from the crystal structure of solid:

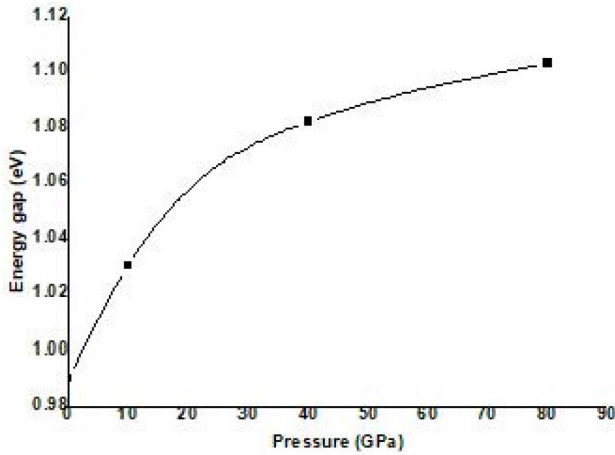


FIGURE 3. Pressure effect on the energy gap of CoNbSn compound.

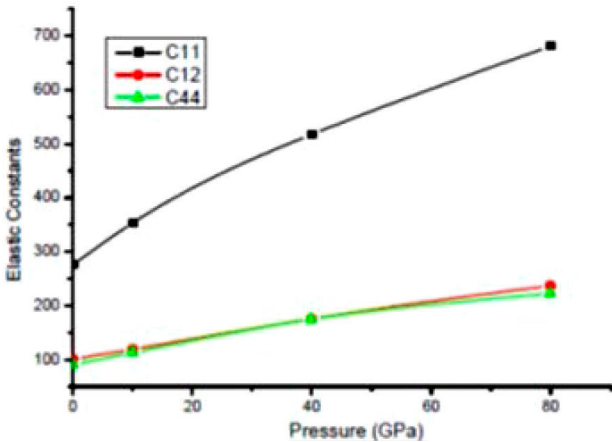


FIGURE 4. Pressure effect on the elastic constants C_{11} , C_{12} , and C_{44} of CoNbSn compound.

The first method is the volume-conserving technique, which is based on analysis of the total energy of the properly strained state of the material. The second method is the stress-strain method, which is based on the analysis of the changes occurring in the calculated stress resulting from the changes in the strain [34]. In the present work, we have used the first method “volume conserving technique” to calculate the second-order elastic constants (C_{ij}).

We investigated the pressure effect on the lattice constant, energy gap, bulk modulus, elastic constants, shear modulus, young modulus, and Poisson ratio for XNbSn ($X = \text{Co, Fe, Cr, Mn, and V}$) alloys at different pressures up to 80 GPa. Table III, displays these parameters at different pressures (0, 10, 40, and 80 GPa) of CoNbSn alloy. By increasing the pressure by 80 GPa, the lattice constant compresses by nearly 7.6%. The value of the energy gap is 0.99 eV at zero pressure and increases slowly to reach 1.103 eV at 80 GPa as shown in Fig. 3. This increase in the value of the energy gap results from increasing the hybridization between the 3d-state of Co atom with the 5s-state of Nb atom.

We calculated the bulk modulus using two methods: first bulk modulus B from the Murnaghan equation, and the second modulus B^* using the elastic constants. Both modulus have a value of 159.019 GPa at zero pressure and become different at higher pressures. From our calculated elastic constants, it can be emphasized the mechani-

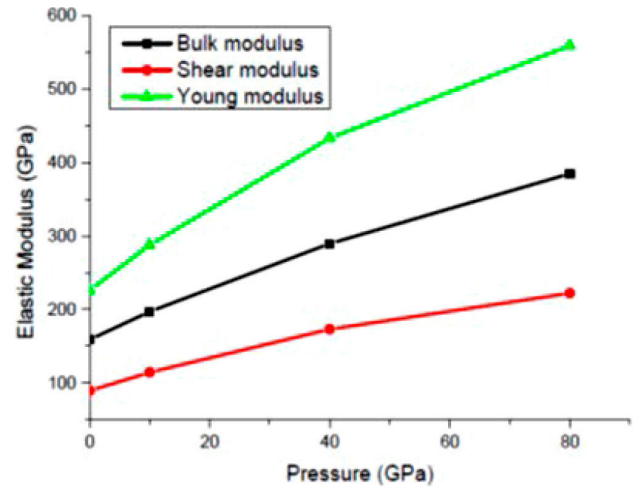


FIGURE 5. Pressure effect on the bulk modulus, shear modulus, and Young's modulus of CoNbSn.

TABLE IV. The lattice constant, bulk modulus, shear modulus, Young modulus, and Poisson ratio ν of FeNbSn compound under different pressures.

Pressure(GPa)	A(A0)	Eg(eV)	B*	C_{11} (GPa)	C_{12} (GPa)	C_{44} (GPa)	B(GPa)	G(GPa)	E(GPa)	ν
0	6.019959	0	161.282	250.23770	116.276380	96.76460	160.93	83.5021	213.568	0.278872
10	5.903745	0	195.375	301.192	137.759	101.029	192.237	92.8036	239.819	0.29208
40	5.807682	0	239.160	363.531	167.1098	107.065	232.584	103.431	270.234	0.306353
80	5.655097	0	321.522	522.102	200.518	154.781	307.713	157.158	402.886	0.281785

cal stability of CoNbSn according to the Born-Huang conditions. We have also studied the variations of elastic constants under different pressures up to 80 GPa as shown in Fig. 4. The elastic constant C_{11} of CoNbSn showed a change of 400 GPa after Applying 80 GPa pressure, while the other constants showed a small variation with pressure. The pressure effect on the bulk modulus, shear modulus, and Young's modulus of CoNbSn is displayed in Fig. 5, where the three moduli increase by increasing the pressure. The Poisson ratio shows a small variation by increasing the pressure. According to Pugh's proposed criterion [35], if a material has a low value of $B/G < 1.75$, then it behaves as brittle material. If $B/G > 1.75$, then this material behaves as ductile material. We have calculated B/G at ambient pressure for CoNbSn(1.779), FeNbSn(1.93), CrNbSn(3.67), and MnNbSn(2.45), which indicate the ductile behavior of these materials.

We present the pressure effect on the lattice constant, bulk modulus, shear modulus, Young modulus, and Poisson ratio (ν) of FeNbSn in Table IV. At zero pressure, the lattice constant of FeNbSn is 6.0199 Å, and it compressed by nearly 6% by applying a pressure of 80 GPa. The elastic constants C_{11} of FeNbSn shows a higher variation than other elastic constants and varies directly by increasing pressure to reach nearly 750 GPa at a pressure of 80 GPa as shown in Fig. 6. The bulk modulus, shear modulus, and Young modulus of

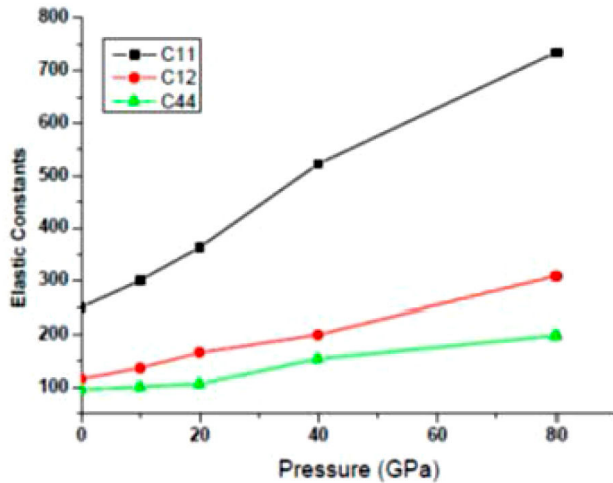
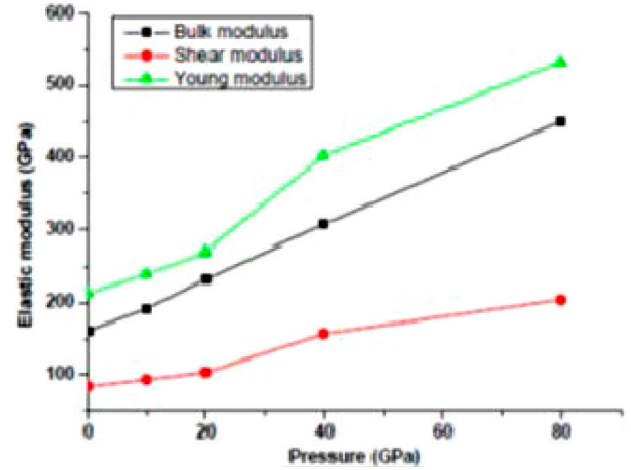
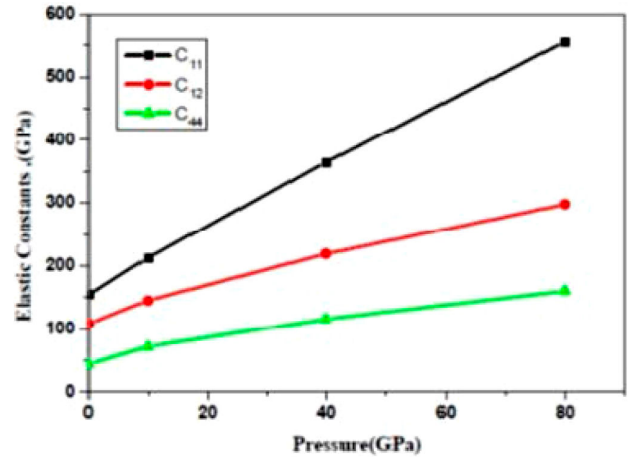

 FIGURE 6. Pressure effect on the elastic constants C_{11} , C_{12} , and C_{44} of FeNbSn compound.


FIGURE 7. Pressure effect on the bulk modulus, shear modulus, and Young's modulus of FeNbSn.


 FIGURE 8. Pressure effect on the elastic constants C_{11} , C_{12} , and C_{44} of CrNbSn compound.

FeNbSn alloy increased by increasing pressure as displayed in Fig. 7. This compound conserves its mechanical stability under higher pressures. This alloy shows a metallic behavior in the pressure range from 0 to 80 GPa. The pressure effect on the lattice constant of CrNbSn is more than other half-Heusler XNbSn alloys. The lattice constant of this alloy decreases by nearly 10% under 80 GPa. The half-Heusler CrNbSn alloy fulfills the conditions of mechanical stability of Born-Huang. The shear and young modulus of CrNbSn

TABLE V. The lattice constant, bulk modulus, shear modulus, Young modulus, and Poisson ratio ν of CrNbSn compound under different pressures.

Pressure(GPa)	A(A0)	E_g (eV)	B*	C_{11} (GPa)	C_{12} (GPa)	C_{44} (GPa)	B(GPa)	G(GPa)	E(GPa)	ν
0	6.176139	0	123.376	154.709064	108.536424	43.689584	123.927	33.8223	93.0057	0.37492
10	6.038825	0	170.868	212.831	144.938	71.326	167.569	52.9453	143.701	0.357073
40	5.768698	0	281.182	364.600	219.091	116.091	267.818	96.1653	257.657	0.339657
80	5.5173	0.409.886	555.075	297.991	160.360	383.686	146.773	390.522	0.330364	

is less than those of other half-Heusler XNbSn alloys (Table V). The dependence of elastic constants on pressure for CrNbSn is shown in Fig. 8, where C_{11} is highly sensitive to high pressure than C_{12} and C_{44} . The elastic moduli of CrNbSn increase by increasing the pressure as shown in Fig. 9. The bulk and shear moduli show more variation with higher pressures than the shear modulus. The values of C_{11} , C_{12} , and C_{44} of MnNbSn increased by a factor of 2.8, 2.2, and 2.17, respectively, by increasing the pressure from 0 GPa

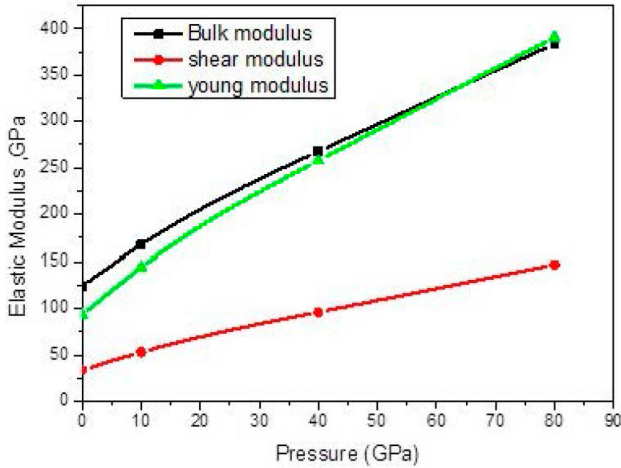


FIGURE 9. Pressure effect on the bulk modulus, shear modulus, and Young's modulus of CrNbSn.

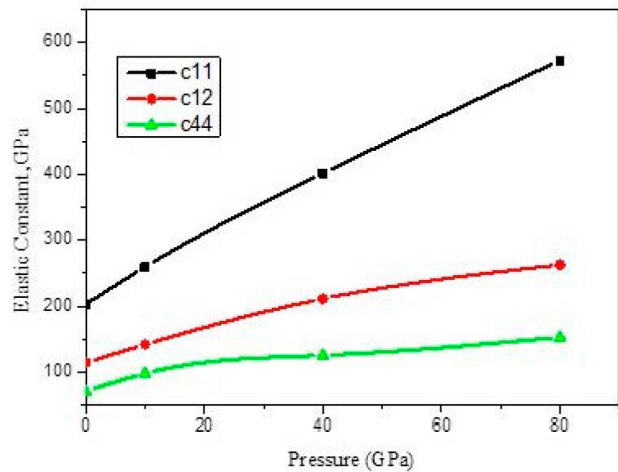


FIGURE 10. Pressure effect on the elastic constants C_{11} , C_{12} , and C_{44} of MnNbSn compound.

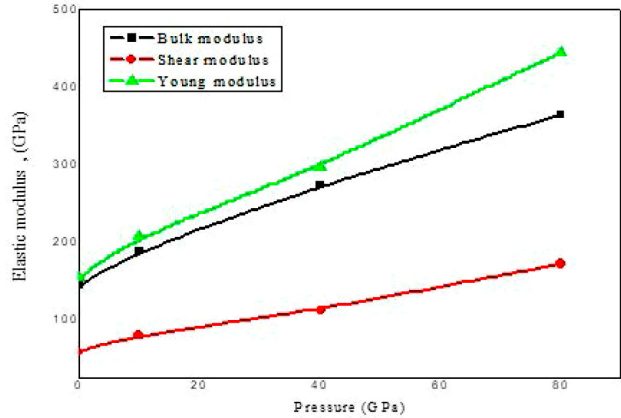


FIGURE 11. Pressure effect on the bulk modulus, shear modulus, and Young's modulus of MnNbSn.

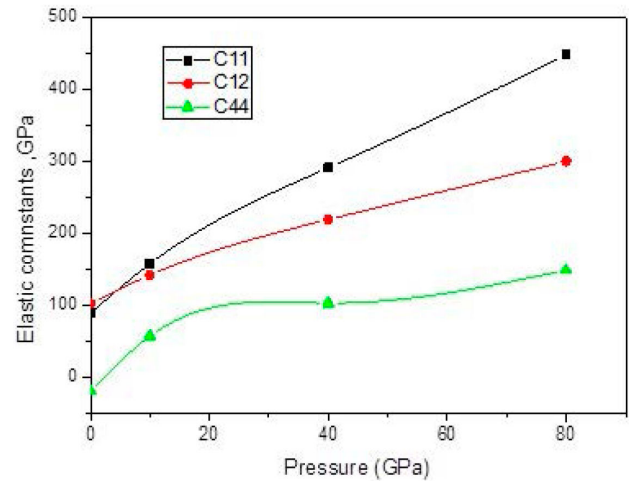


FIGURE 12. Pressure effect on the elastic constants C_{11} , C_{12} , and C_{44} of VNbSn compound.

to 80 Gpa. The condition of mechanical stability is found under all pressure values. Figure 10 displays the pressure effect on the elastic constants C_{11} , C_{12} , and C_{44} of MnNbSn compound. It is clear the three constants increase by increasing pressure, while C_{11} is more sensitive to pressure than the C_{12} and C_{44} constants. The Pressure effect on the bulk modulus, shear modulus, and Young modulus of MnNbSn is displayed in Fig. 11. Table VI displays the lattice constant, bulk modulus, shear modulus, Young modulus, and Poisson ratio of MnNbSn compound under different pressures. The pres-

TABLE VI. The lattice constant, bulk modulus, shear modulus, Young modulus, and Poisson ratio ν of MnNbSn compound under different pressures.

Pressure(GPa)	A(A0)	Eg(eV)	B*	C_{11} (GPa)	C_{12} (GPa)	C_{44} (GPa)	B(GPa)	G(GPa)	E(GPa)	ν
0	6.0861	0	143.679	202.937	114.219	70.138	143.791	58.3677	154.234	0.321229
10	5.964	0	183.859	259.279	141.699	97.848	188.892	79.7647	208.629	0.307778
40	5.741165	0	286.286	401.716	211.041	125.339	274.599	112.332	296.558	0.320006
80	5.571816	0	387.510	573.178	262.533	152.803	366.082	153.806	404.735	0.315735

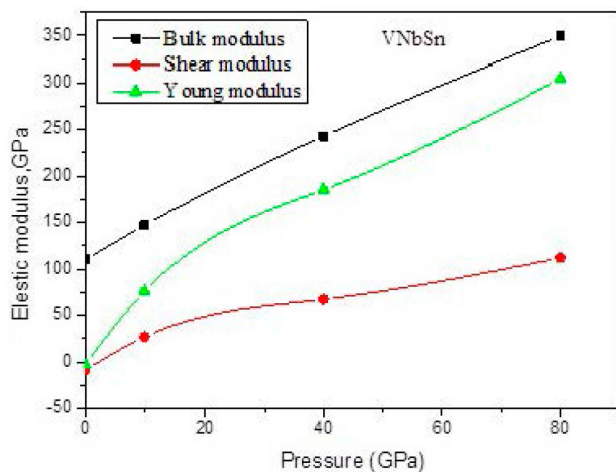


FIGURE 13. Pressure effect on the bulk modulus, shear modulus, and Young's modulus of VNbSn.

sure effect on the elastic constants of VNbSn is displayed in Fig. 12. It shows a strange behavior, where at zero pressure $C_{12} > C_{11}$, and at 4 GPa this behavior is reversed $C_{11} > C_{12}$. According to this behavior, we guess that a phase change occurs at nearly 4 GPa pressure and this compound becomes stable and satisfy the stability conditions under hydrostatic pressure. The C_{44} elastic constant should be positive, but it results negative at lower pressures (from 0 to 4 GPa). We think it is a sign of the structure having a broken symmetry below 4 GPa and the energy of the crystal being lower than the energy of cubic structure. We hope in the future, the presence of more studies about these interesting compounds using different calculations methods. Pressure

effect on the bulk modulus, shear modulus, Young modulus, and Poisson ratio of VNbSn is shown in Fig. 13. The lattice constant, bulk modulus, shear modulus, Young modulus, and Poisson ratio of VNbSn compound under different pressures are displayed in Table VI. The bulk modulus increases by nearly 264 GPa by increasing the pressure by 80 GPa. The Poisson ratio decreases by increasing the pressure. For all the studied compounds, the Poisson's ratio at zero GPa is more than 0.26, which confirms the ductility of these materials. For all the studied compounds, except VNbSn at 0 GPa, we found that $(C_{11} > C_{12} > C_{44})$ indicating the high resistance of these compounds to linear compression along α axis under hydrostatic pressure. The condition of stability $C_{11} > C_{12}$ is not met at zero pressure, while at higher pressure it is fulfilled. All other stability conditions were met under all pressures.

4. Conclusion

We have performed first-principles calculations to investigate the structural and elastic properties of the half-Heusler XNbSn (X = Cr, Mn, Co, Fe, V) alloys in the ferromagnetic state FM. The elastic constants and elastic moduli are investigated under different pressures (0, 20, 40, and 80 GPa). These hypothetical half-Heusler alloys show a mechanical stability under higher pressure up to 80 GPa. All the studied alloys show a metallic characteristic except CoNbSn which shows a semiconductor behavior with energy gap of 0.99 eV. The pressure effect on the elastic constants of these compounds was investigated. We predicted that C_{11} constant is highly more sensitive to high pressure than C_{12} and C_{44} .

1. T. Gottschall, E. Stern-Taulats, L. Maosa, A. Planes, and K.P. Skokov, Reversibility of minor hysteresis loops in magnetocaloric Heusler alloys. *Appl. Phys. Lett.* **110** (2017) 223904, <https://doi.org/10.1063/1.4984797>.
2. R. Masrour, A. Jabar, and E. K. Hlil, Modeling of the magnetocaloric effect in Heusler Ni2MnGa alloy: Ab initio calculations and Monte Carlo simulations. *Intermetallics*, **91** (2017) 120, <https://doi.org/10.1016/j.intermet.2017.08.012>.
3. Y. Chieda, T. Kanomata, K. Fukushima, K. Matsubayashi, Y. Uwatoko, and R. Kainuma, Magnetic properties of Mn-rich Ni2MnSn Heusler alloys under pressure. *J. Alloys Compd.* **486** (2009) 55, <https://doi.org/10.1016/j.jallcom.2009.06.206>.
4. B. M. Wang *et al.*, Strong thermal-history-dependent magnetoresistance behavior in Ni49.5Mn34.5In16. *J. Appl. Phys.* **106** (2009) 063909, <https://doi.org/10.1063/1.3225578>.
5. S. H. Aly, and R. M. Shabara, First principles calculation of elastic and magnetic properties of Cr-based full-Heusler alloys. *J. Mag. and Mag. Mat.*, **360** (2014) 143, <https://doi.org/10.1016/j.jmmm.2014.02.030>.

6. R. M. Shabara and B. O. Alsobhi, Calculations of structural, elastic and magnetic properties of the novel full Heusler alloys Ru2XY (X = Nb, Mn) and (Y = Te, Sb), *JETP Lett.* **113** (2021) 322, <https://doi.org/10.1134/S0021364021050015>.
7. R. M. Shabara, High pressure effect on structural, electronic and elastic properties of topological half-Heusler LaPdBi compound. *Mater. Res. Express*, **4** (2017) 086511, <https://doi.org/10.1088/2053-1591/aa84be>.
8. A. G. Kiiamov, M. D. Kuznetsov, R. G. Batulin, and D. A. Tayurskii, On the ab initio Calculations within DFT+U Approach of Physical Properties of a Compound with Strong Electron-Electron Correlations by the Case of KFeS2. *JETP Lett.* **115** (2022) 98, <https://doi.org/10.1134/S0021364022020023>.
9. A. Bouazza, M. Khirat, M. Larbi, N. Bettaher, and D. Rached, Structural, mechanical, electronic, thermal, and optical properties of the inverse-Heusler compounds X2RuPb (X = La, Sc): A first-principles investigation. *Rev. Mex. Fis.* **69** (2023) 050501, <https://doi.org/10.31349/RevMexFis.69.050501>.
10. R. J. Quinn, and J. W. G. Bos, Advances in half-Heusler alloys for thermoelectric power generation. *Materials advances*, **2** (2021) 6246, <https://doi.org/10.1039/D1MA00707F>.
11. A. Q. Seh, and D. C. Gupta, Quaternary Heusler Alloys a Future Perspective for Revolutionizing Conventional Semiconductor Technology. *J. alloys and Comp*, **871** (2021) 159560, <https://doi.org/10.1016/j.jallcom.2021.159560>.
12. H. Ohno, Making nonmagnetic semiconductors ferromagnetic. *Science*, **281** (1998) 951, <https://doi.org/10.1126/science.281.5379.951>.
13. M. Jimbo, S. Hirano, K. Meguro, S. Tsunashima and S. Uchiyama, Giant Magnetoresistance with Low Saturation Field in Ni14Fe13Co73/Cu Multilayers. *Jpn. J. Appl. Phys.* **33** (1994) 850, <https://doi.org/10.1143/JJAP.33.L850>.
14. S. Mitani, Magnetic Tunnel Junctions Using Heusler Alloys. In: Felser, C., Hirohata, A. (eds) Heusler Alloys. *Springer Series in Materials Science*, vol **222**. (Springer, Cham, 2016).
15. S. Okamura, A. Miyazaki, S. Sugimoto, N. Tezuka, and K. Inomata, Large tunnel magnetoresistance at room temperature with a Co2FeAl full-Heusler alloy electrode. *Appl. Phys. Lett.* **86** (2005) 232503, <https://doi.org/10.1063/1.1944893>.
16. T. Kubota, Y. Ina, Z. Wen, and K. Takanashi, Temperature dependence of current-perpendicular-to-plane giant magnetoresistance in the junctions with interface tailored Heusler alloy electrodes, *J. Magn. Magn. Mat* **474** (2019) 365, <https://doi.org/10.1016/j.jmmm.2018.11.051>.
17. B. Yan, and A. de Visser, Half-Heusler topological insulators. *MRS Bulletin*, **39** (2014) 859, <https://doi.org/10.1557/mrs.2014.198>.
18. T. Graf *et al.*, Phase-separation-induced changes in the magnetic and transport properties of the quaternary Heusler alloy Co2Mn1-xTixSn. *Scr. Mater.* **63** (2010) 1216, <https://doi.org/10.1103/PhysRevB.82.104420>.
19. A. Roy, J. W. Bennett, K. M. Rabe and D. Vanderbilt, Half-Heusler Semiconductors as Piezoelectrics. *Phys. Rev. Lett.* **109** (2012) 037602, <https://doi.org/10.1103/PhysRevLett.109.037602>.
20. D. Kieven, R. Klenk, S. Naghavi, C Felser and T. Gruhn, I-II-V half-Heusler compounds for optoelectronics: Ab initio calculations. *Phys. Rev. B*, **81** (2010) 075208, <https://doi.org/10.1103/PhysRevB.81.075208>.
21. W. Li, G. Yang, and J. Zhang, Optimization of the thermoelectric properties of FeNbSb-based half-Heusler materials. *J. Physics D: Applied Phys*, **49** (2016) 195601, <https://doi.org/10.1088/0022-3727/49/19/195601>.
22. A. A. Musari, Electronic, mechanical, vibrational and thermodynamic properties of FeXSb (X = Hf and Nb) Half-Heusler alloys from first-principles approach. *Solid State Sciences*, **122** (2021) 106755, <https://doi.org/10.1016/j.solidstatesciences.2021.106755>.
23. D. K. Yadav, S. R. Bhandari, and G. C. Kaphle, Structural, elastic, electronic, and magnetic properties of MnNbZ (Z = As, Sb) and FeNbZ (Z = Sn, Pb) semi-Heusler alloys. *Mater. Res. Express*, **7** (2020) 116527, <https://doi.org/10.1088/2053-1591/abcc86>.
24. E. L. Habbak, R. M. Shabara, S. H. Aly, and S. Yehia, Investigating half-metallicity in PtXSb alloys (X=V, Mn, Cr, Co) at ambient and high pressure. *Physica B: condensed Matter* **494** (2016) 63, <https://doi.org/10.1016/j.physb.2016.04.009>.
25. J. P. Perdew, Density-functional approximation for the correlation energy of the inhomogeneous electron gas. *Phys. Rev. B*, **33** (1986) 8822, <https://doi.org/10.1103/PhysRevB.33.8822>.
26. D. C. Langreth, and J.P. Perdew, Theory of nonuniform electronic systems. *Phys. Rev. B*, **21** (1980) 5469, <https://doi.org/10.1103/PhysRevB.21.5469>.
27. R. G. Parr, S. R. Gadre, and L. J. Bartolotti, Local density functional theory of atoms and molecules, *Proc. Natl. Acad. Sci.* **76** (1979) 2522, <https://doi.org/10.1073/pnas.76.6.2522>.
28. S. Lundqvist, N. H. March, Theory of the Inhomogeneous Electron Gas, Plenum, (New York, 1983).
29. P. Blaha, K. Schwarz, P. I. Sorantin and S. B. Trickey, Full-potential, linearized augmented plane wave programs for crystalline systems. *Comput. Phys. Commun.* **59** (1990) 399, [https://doi.org/10.1016/0010-4655\(90\)90187-6](https://doi.org/10.1016/0010-4655(90)90187-6).
30. F. D. Murnaghan, The Compressibility of Media under Extreme Pressures. *Acad. Sci.* **30** (1944) 244, <https://doi.org/10.1073/pnas.30.9.244>.
31. F. Birch, Finite Elastic Strain of Cubic Crystals. *Phys. Rev.* **71** (1947) 809, <https://doi.org/10.1103/PhysRev.71.809>.
32. J. Wang, S. Yip, S. R. Phillpot, and D. Wolf, Crystal instabilities at finite strain. *Phys. Rev. Lett.* **71** (1993) 4182, <https://doi.org/10.1103/PhysRevLett.71.4182>.
33. M. Born and K. Huang, Dynamical Theory of Crystal Lattices (Clarendon Press, Oxford, 1956).

34. B. Mayer, H. Anton, E. Bott, M. Methfessel, J. Sticht, and P. Schmidt, Ab-initio calculation of the elastic constants and thermal expansion coefficients of Laves phases. *Intermetallics*, **11** (2003) 23, [https://doi.org/10.1016/S0966-9795\(02\)00127-9](https://doi.org/10.1016/S0966-9795(02)00127-9).
35. S. Pugh, The London, Edinburgh, and Dublin, Relations between the Elastic Moduli and the Plastic Properties of Polycrystalline Pure Metals. *Philosophical Magazine and Journal of Science*, **45** (1954) 823, <https://doi.org/10.1080/14786440808520496>.